Effects of turbulence model in computational fluid dynamics of horizontal axis wind turbine aerodynamic

Kamyar Mansour, Mohsen Yahyazade
Department of Aerospace Engineering
Amirkabir University of Technology
Hafez Avenue, Tehran, 15875-4413
IRAN
mansour@aut.ac.ir

Abstract: - The present paper report the numerical solution of horizontal axis wind turbines (HAWTs) of the aerodynamics with used of computational fluid dynamics, CFD with three different turbulent models, and compare these turbulence model results with experimental data to validate and determine more reliable numerical solutions. Computational domain was divided in two zones; rotating and stationary .The numerical solution was carried out in the rotation zone, by solving conservation equations in a rotating reference frame. The blades have fixed 12° pitch angle and the computational results for different turbulent models such as standard k-ε, RNG k-ε & Spalart- Allmaras has been reported and compare with the experimental data of The National Renewable Energy Laboratory (NREL), for two wind speeds. It seems that the one-equation Spalart-Allmaras model is the suitable for turbulence closure, in low wind speed, and RNG k-ε model is more reliable for higher wind speed.

Key-Words: - Wind turbine, HAWT, turbulence model, pressure coefficient, NREL, blade torque

1 Introduction

Numerical solution of flows through wind turbines is increasingly useful since it helps reduce time and cost in wind turbine development and usually the flow around wind turbine blades is turbulent, with the whole or part of the blade very often operating under stall conditions, thus turbulence model is increasingly important in numerical analysis of the horizontal axis wind turbine. As you know there is no single turbulence model to be universally accepted as being superior for all classes of problems. The choice of turbulence model will depend on considerations such as the physics encompassed in the flow, the established practice for a specific class of problem.

Flow pass an untwisted HAWT blade is too much complex because it combined of axial inflow velocity at the rotor plane the inflow velocity caused by the rotation of the blade, and the inflow velocity caused by wake rotation at the rotor plane. In addition, centrifugal force acting along the blade due to the rotation of the blade, cause a flow along the span.[1-3]

Wind speed is constant and as blade radius increase along the span of blade then annular velocity, rw, increase linearly. So, the angle of attack is change either and this cause the change in lift and drag orientation. As approached hub annular velocity increase, then angle of attack decrease and flow on the upper surface of the airfoil begins to separate and a condition known as stall begins to develop in the we have stall there;

Another subject that involved with HAWT blade is grid generation. Because of the low Reynolds number in wind turbine, boundary condition is important in numerical analysis of HAWT blade, thus rectangular mesh near the blade is more efficient. We point out that matching the full structure rectangular mesh with the periodic boundary condition is too difficult.

In this study, rotating wind turbine modeled with rotating reference frame instead of dynamic grid so the model could be solved steady.

2 Problem Formulation

The solution has been done in pressure base that the pressure equation is derived from the continuity and the momentum equations. In this approach the velocity field, corrected by the pressure, satisfies the continuity.

Second-order accuracy is desired in momentum equation upwind discretization. Quantities at cell faces are computed using a multidimensional linear reconstruction approach [4]. In this approach, Taylor series expansion has been employed to achieve higher-order accuracy.

The quick scheme is used in order to compute a higher-order value of the convected variable at a face [5]. This scheme are based on a weighted average of second-order-upwind and central interpolations of the variable
The quick scheme has much accuracy in structured meshes.
The simple algorithm is employed to couple velocity and pressure. This algorithm uses a relationship between velocity and pressure corrections to enforce mass conservation and to obtain the pressure field.

2.1 Governing equations:

Momentum equation [6]

$$\frac{\partial \rho \overrightarrow{U_r}}{\partial t} + \nabla.\left(\rho \overrightarrow{U_r}\overrightarrow{U_r}\right) + 2\rho\vec{\omega} \times \overrightarrow{U_r} + \rho\vec{\omega} \times (\vec{\omega} r) = \vec{\nabla}.\sigma \quad (1)$$

Where, $\overrightarrow{U_r}$, is relative velocity, $\vec{\omega}$ is rotational velocity, $2\rho\vec{\omega} \times \overrightarrow{U_r}$ is the Coriolis force and $\rho\vec{\omega} \times (\vec{\omega} r)$ is centrifugal force; $\boldsymbol{\sigma}$ is the stress tensor of a Newtonian fluid. According to the eddy viscosity concept in turbulence modeling, $\boldsymbol{\sigma}$ can be represented as:

$$\sigma = -\left(\mathrm{P} + \frac{2}{3}\mu_{\mathrm{eff}}\nabla.\overrightarrow{U_r}\right)\mathrm{I} + \mu_{\mathrm{eff}}\left[\vec{\nabla}\overrightarrow{U_r} + \left(\vec{\nabla}\overrightarrow{U_r}\right)^{\mathrm{T}}\right]$$

Where $\mu_{\mathrm{eff}} = \mu + \mu_{\mathrm{t}}$
μ_{t} is the eddy viscosity that can be calculated from a turbulence mode.

2.2. Turbulence models:

The governing equation that has been used for three turbulence model that we use in numerical solution, in explained below.

2.1.1 Spalart-Allmaras model:

The Spalart-Allmaras model is a rather simple one-equation model. It can solve transport equation that is modeled for the kinematic turbulent viscosity. The Spalart-Allmaras model was designed specifically for aerospace applications involving wall-bounded flows and has been shown to give good results for boundary layers subjected to adverse pressure gradients. It is also has good results in the turbo machinery applications.
In fact, the Spalart-Allmaras model is effectively a low-Reynolds-number model that has the viscosity-affected region of the boundary layer. Furthermore, in Spalart-Allmaras turbulence model the near-wall gradients of the transported variable are much smaller than the gradients of the transported variables in the k-ε or k-w models so it's not much sensitive to numerical errors when unstructured meshes are used near walls.[7]
The transported variable in the Spalart-Allmaras model, $\tilde{v}$, is identical to the turbulent kinematic viscosity except in the near-wall (viscosity-affected) region. The transport equation for $\tilde{v}$ is [7]:

$$\frac{\partial}{\partial t}(\rho\tilde{v}) + \nabla.(\rho\tilde{v}u_i) = G_{\tilde{v}} + \frac{1}{\sigma_{\tilde{v}}}\{\nabla.[(\mu + \rho\tilde{v})\nabla\tilde{v}] + C_{b2}(\nabla\tilde{v})^2\} - Y_{\tilde{v}} \quad (3)$$

The quantity $\mathrm{Y}_{\tilde{v}}$ is the destruction of turbulent viscosity that occurs in the near wall region due to wall blocking and viscous damping. The quantities $\sigma_{\tilde{v}}$ and $\mathrm{C}_{\mathrm{b}2}$ are the constants and v is the molecular kinematic viscosity of course, u_i is the components of relative velocity $\overrightarrow{U_r}$.
The turbulent viscosity, μ_{t}, is computed as equation:

$$\mu_{\mathrm{t}} = \rho\tilde{v}\mathrm{f}_{v1} \quad (4)$$

Where the viscous damping factor f_v is expressed by

$$f_{v1} = \frac{x^3}{x^3 + C_{v1}^3} \quad (5)$$

The quantity x relates the transport variable and the molecular kinematic viscosity

$$\mathrm{x} = \frac{\tilde{v}}{v} \quad (6)$$

G_v is the production of turbulent viscosity modeled as:

$$\mathrm{G}_v = \mathrm{C}_{\mathrm{b}1}\rho\tilde{\mathrm{S}}\tilde{v} \quad (7)$$

Where

$$\tilde{S} \equiv S + \frac{\tilde{v}}{k^2 d^2} f_{v2} \quad (8)$$

And

$$f_{v2} = 1 - \frac{x}{1 + x f_{v1}} \quad (9)$$

The quantities $\mathrm{C}_{\mathrm{b}1}$ and k are constants, d is the distance from the wall, and S is a scalar measure of the deformation tensor. S is based on the magnitude of the vorticity:

$$S \equiv \sqrt{2\Omega_{ij}\Omega_{ij}} \quad (10)$$

Where Ω_{ij} is the mean rate-of-rotation tensor and is defined by

$$\Omega_{ij} = \frac{1}{2}\left(\frac{\partial u_i}{\partial x_j} - \frac{\partial u_j}{\partial x_i}\right) \quad (11)$$

The destruction term is modeled as:

$$Y_v = C_{w1}\rho f_w \left(\frac{\tilde{v}}{d}\right)^2 \quad (12)$$

Where

$$f_w = g\left[\frac{1 + C_{w3}^6}{g^6 + C_{w3}^6}\right]^{1/6} \quad (13)$$

$$g = r + C_{w2}(r^6 - r) \quad (14)$$

$$r \equiv \frac{\tilde{v}}{\tilde{S}k^2d^2} \quad (15)$$

Cw1, Cw2, and Cw3 are constants.
From the Spalart-Allmaras model the values for the eight constants were determined from experimental data as:

$$C_{b1} = 0.1355 \qquad C_{b2} = 0.622 \qquad \sigma_{\tilde{v}} = \frac{2}{3}$$

$$C_{v1} = 7.1 \qquad C_{w2} = 0.3 \qquad C_{w3} = 2.0$$

$$k = 0.418 \qquad C_{b1} = \frac{C_{b1}}{k^2} + \frac{(1 + C_{b2})}{\sigma_{\tilde{v}}} \quad (16)$$

2.2.2 Standard k-ε model:
The simplest "complete models" of turbulence are the two-equation models in which the solution of two separate transport equations allows the turbulent velocity and length scales to be independently determined. The standard k-ε model falls within this class of models.
It is the most widely used model but it cannot predict flow separation accurately because it neither integrates up to the wall nor does it account for modification of turbulence dissipation due to an adverse pressure gradient.
It is a semi-empirical model, and the derivation of the model equations relies on phenomenological considerations and empiricism. The standard k-ε model is a semi-empirical model based on model transport equations for the turbulence kinetic energy (k) and its dissipation rate (ε). The model transport equation for k is derived from the exact equation, while the model transport equation for ε was obtained using physical reasoning and bears little resemblance to its mathematically exact counterpart.
In the derivation of the k-ε model, the assumption is that the flow is fully turbulent, and the effects of molecular viscosity are negligible. The standard k-ε model is therefore valid only for fully turbulent flows. [8, 9, 10]

$$\frac{\partial}{\partial t}(\rho k) + \nabla.(\rho k U) = \nabla.\left[\left(\mu + \frac{\mu_t}{\sigma_k}\right)\nabla k\right] + \tau_{ij}\nabla U - \rho\varepsilon \quad (17)$$

$$\frac{\partial}{\partial t}\varepsilon + \nabla.(\rho\varepsilon U) = \nabla.\left[\left(\mu + \frac{\mu_t}{\sigma_\varepsilon}\right)\nabla k\right] + C_{1\varepsilon}\frac{\varepsilon}{k}\tau_{ij}\nabla U - C_{2\varepsilon}\rho\frac{\varepsilon^2}{k} \quad (18)$$

Where, τ_{ij} is the Reynolds stress tensor. By applying the Boussinesq's hypothesis, τ_{ij} , is linearly related to the mean flow strain tensor:

$$\tau_{ij} = \mu_t\left[\nabla U + (\nabla U)^T - \left(\frac{2}{2}\nabla.U\right)I\right] + \frac{2}{2}\rho k I \quad (19)$$

The turbulent (or eddy) viscosity, μ_t , is computed by combining k and ε as follows

$$\mu_t = \rho C_\mu \left(\frac{k^2}{\varepsilon}\right) \quad (20)$$

From the standard k-ε model the values for the five constants were determined from experimental data as [8]

$$C_\mu = 0.09 \qquad C_{1\varepsilon} = 0.09 \qquad C_{2\varepsilon} = 1.92$$
$$\sigma_k = 1.0 \qquad \sigma_\varepsilon = 1.3 \quad (21)$$

2.2.3. RNG k-ε Model:
The RNG k-ε model was derived using a statistical technique called renormalization group theory. It is similar in form to the standard k-ε model, but it accurate and reliable for a wider class of flows than the standard k-ε model. And also the RNG model is more responsive to the effects of rapid strain and streamlines curvature than the standard k-ε model [10]
Governing equation for transport equations k and ε are:

$$\frac{\partial}{\partial t}(\rho k) + \nabla.(\rho k U) = \nabla.[\propto_k \mu_{eff}\nabla k] + \tau_{ij}\nabla U - \rho\varepsilon \quad (22)$$

$$\frac{\partial}{\partial t}\varepsilon + \nabla.(\rho\varepsilon U) = \nabla.[(\propto_\varepsilon \mu_{eff}\nabla\varepsilon)]$$

$$+C_{1\varepsilon}\frac{\varepsilon}{k}\tau_{ij}\nabla U - C_{2\varepsilon}\rho\frac{\varepsilon^2}{k} - R_\varepsilon \quad (23)$$

τ_{ij} and μ_t are calculated as standard k-ε model in equations (19) and (20) .
The inverse effective Prandtl numbers, $\propto_k$ and $\propto_\varepsilon$, are computed using the following formula derived analytically by the RNG theory:

$$\left|\frac{\propto -1.3929}{\propto_0 - 1.3929}\right|^{0.6321}\left|\frac{\propto -2.3929}{\propto_0 - 2.3929}\right|^{0.3679} = \frac{\mu_{mol}}{\mu_{eff}} \quad (24)$$

Where $\propto_0 = 1$. In the high-Reynolds-number limit

$\left(\mu_{mol}/\mu_{eff} \ll 1\right)$, $\propto_k = \propto_\varepsilon = 1.393$

The main difference between the RNG and standard k-ε models lies in the additional term in the ε equation given by

$$R = \frac{C_\mu \rho \eta^3 (1 - \eta/\eta_{\eta_0})}{1 + \beta\eta^3}\frac{\varepsilon^2}{k} \quad (25)$$

Where

$$\eta \equiv \frac{Sk}{\varepsilon} \quad , \quad \eta_0 = 4.38 \quad , \beta = 0.012 \quad (26)$$

Equation 23 can be rearranged by using equation 25, so that the third and fourth terms on the right-hand side of Equation 23 can be merged, and the resulting ε equation can be rewritten as:

$$\frac{\partial}{\partial t}\rho\varepsilon + \nabla.(\rho\varepsilon U) = \nabla.[(\propto_\varepsilon \mu_{eff}\nabla\varepsilon)] + C_{1\varepsilon}\frac{\varepsilon}{k}\tau_{ij}\nabla U - C^*_{2\varepsilon}\rho\frac{\varepsilon^2}{k} - R_\varepsilon \quad (27)$$

Where $C^*_{2\varepsilon}$ is given by

$$C^*_{2\varepsilon} \equiv C_{2\varepsilon} + \frac{C_\mu \eta^3 (1 - \eta/\eta_0)}{1 + \beta\eta^3} \quad (28)$$

Constants in RNG k-ε model are:

$$C_{1\varepsilon} = 1.42 \qquad C_{2\varepsilon} = 1.68$$
$$\eta = 3 \qquad C^*_{2\varepsilon} = 2 \quad (29)$$

2.3. Grid generation and rotation model:

In this study we divided the domain in two zones in domain that is shown in fig.1 one zone is attached to the rotor blades blade and equations are solved in a Moving Reference Frame (MRF) in this zone. And another zone in away from rotor blades equations are solved stationary.

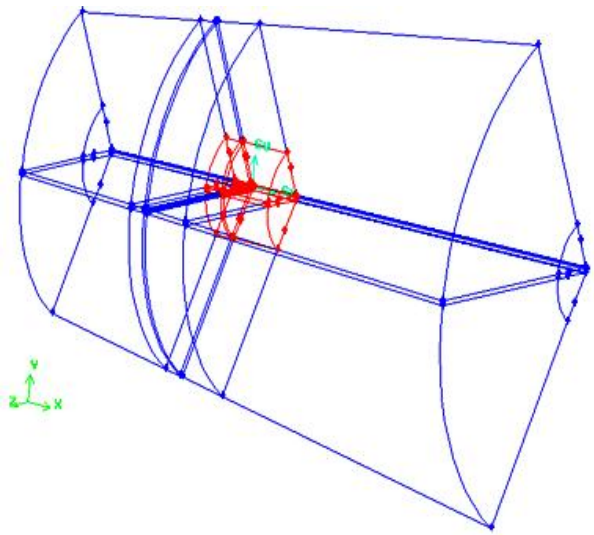

Fig.1 Computational domain zones [14]

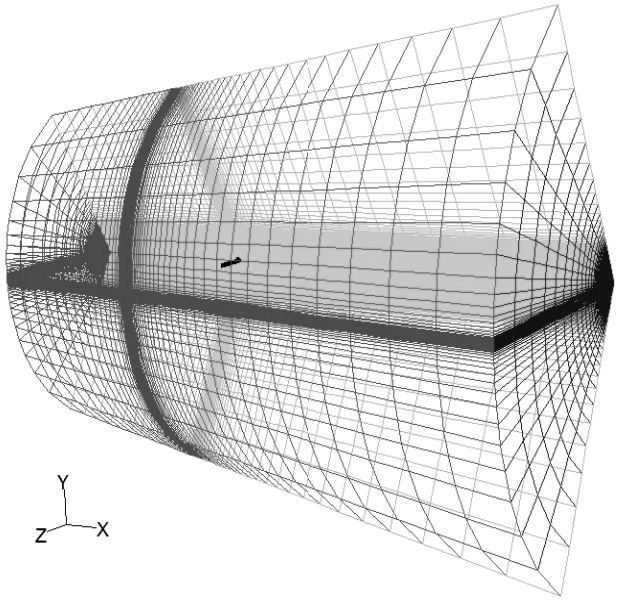

Fig.2 Computational domain

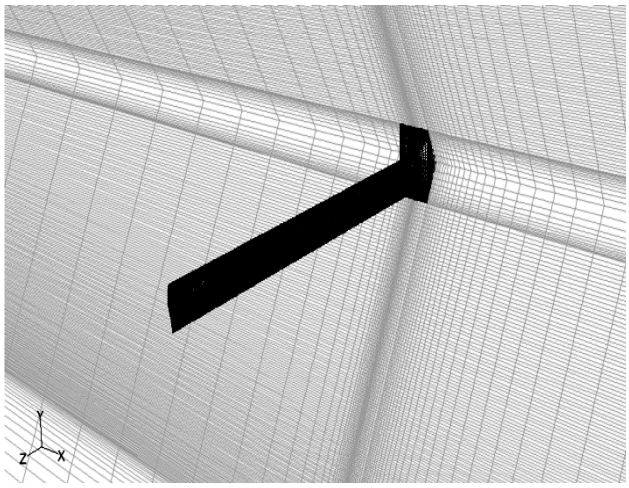

Fig.3 Sidelong view of blade with periodic condition

With used of a moving reference frame in CFD solution, it is possible to solve the problem which is unsteady in the stationary frame in steady with respect to the moving frame. [11]

The fluid velocities can be transformed from the stationary frame to the rotating frame using the following relation:

$$\overrightarrow{V_r} = \vec{V} - \overrightarrow{U_r} \quad (30)$$

Where

$$\overrightarrow{U_r} = \vec{\omega} \times \vec{r} \quad (31)$$

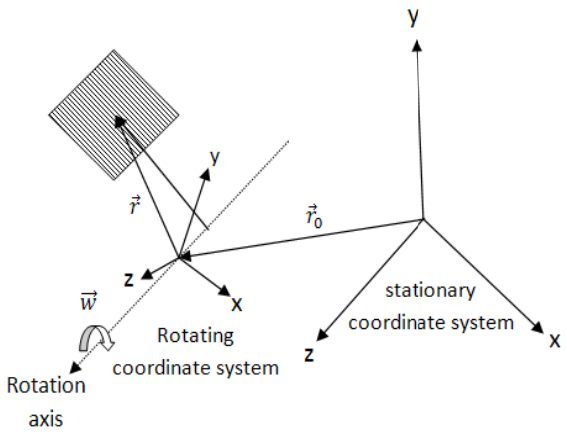

Fig. 4 Rotating Reference Frames in view of Stationary Reference Frames

Where,$\overrightarrow{V_r}$ is the the velocity viewed from the rotating frame, called relative velocity, $\vec{V}$ is the velocity viewed from the stationary frame called the absolute velocity, and $\overrightarrow{U_r}$ is the "whirl" velocity due to the rotating coordinate system.

Fig.2 show the computational domain of the grid in several view are shown in fig4-7. As shown in fig.2 and fig.3 , the solution have been done for only one third domain include one blade, and use periodic boundary condition in order to account for all tree blade with full domain. Grid is rectangular for faces and hexahedral for 3D volume, because this kind of grid has high accuracy in the computation especially in low Reynolds number that boundary layer is important. To see boundary layer better, grid approach the blade is tine (fig.5 and fig.6).

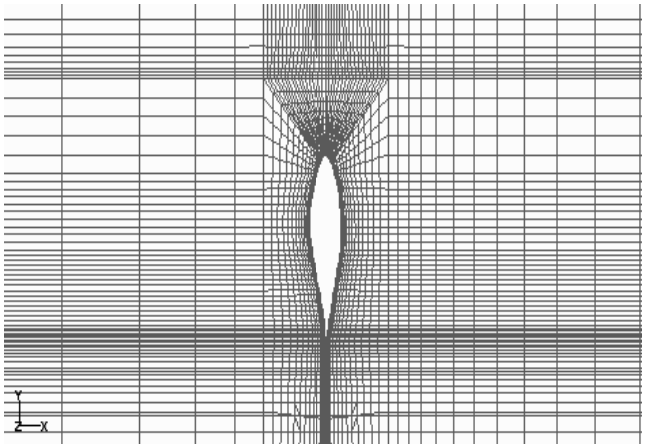

Fig.5 Grid for the blade section airfoil.

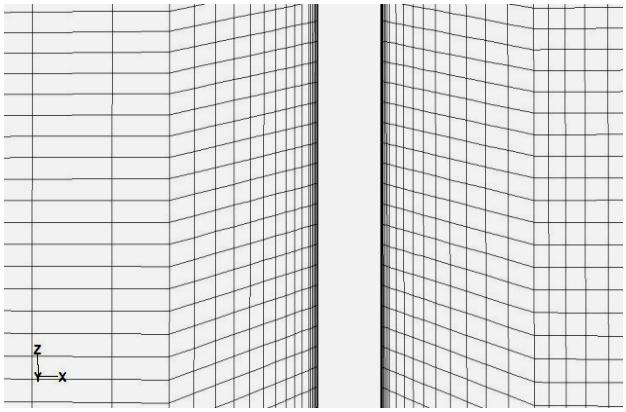

Fig.6 Grid along of the blade span

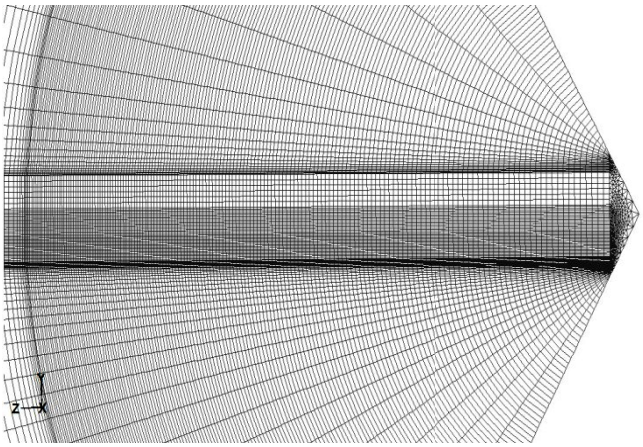

Fig.7 Side view of computational domain mesh

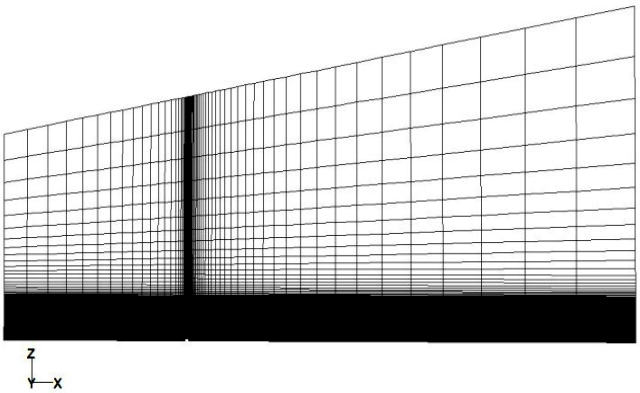

Fig.8 Sectional view of computational domain mesh.

2.4 Wall Yplus value for turbulence models:

Resolution of the mesh and the Reynolds number of the flow, are tow parameters that determined the values of Yplus are defined only in cells attached to the wall. The value of y+ in the wall-adjacent cells dictates how wall shear stress is calculated.
The equation for Yplus is:

$$y^+ = \frac{y}{\mu}\sqrt{\rho\tau_w} \qquad (32)$$

Where y is the distance from the wall to the cell center, μ is the molecular viscosity, ρ is the density of the air, and τ_w is the wall shear stress.
When turbulence model is used to solve CFD model, the wall Yplus of the cells attached the wall should be very small on the order approximately 30 or greater.
Fig.9 and fig.10 indicates that, Regardless of turbulence model, wall Yplus is between 30 and 150for much of these regions it does not drop significantly below 30, except for a few small regions in trailing edge. Therefore it can be concluded that the near-wall mesh resolution is acceptable.

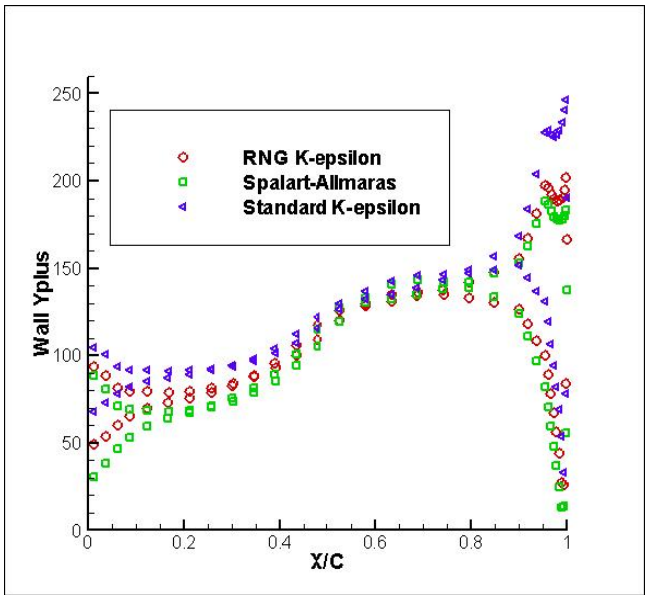

Fig.9 Wall Yplus around blade section in 80% span at 10.5 m/s wind speed

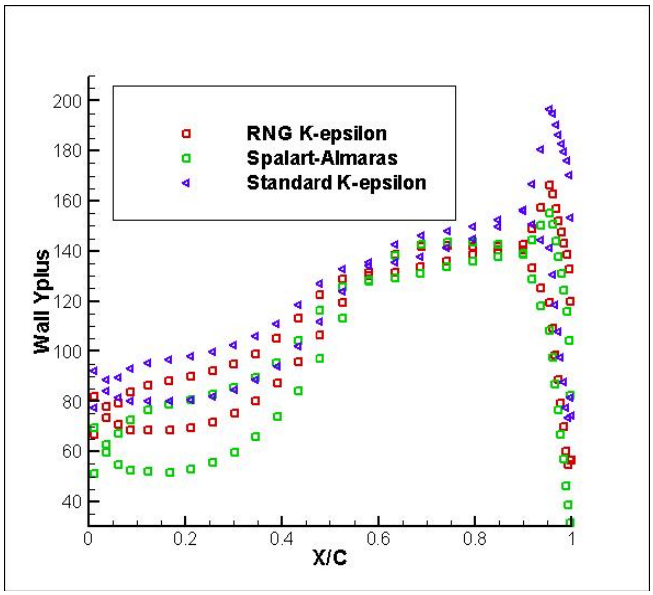

Fig.10 Wall Yplus around blade section in 80% span at 7.2 m/s wind speed

3 Problem Solution

Over the past recent years, under the support of the National Renewable Energy Laboratories, work has been underway on the development of several different wind turbines experimental test in wind tunnel and made available documented and experimental field data to use in several researches. In this study NREL Phase II Wind Turbine available

test data have been used to validate the numerical result [9, 12]. In this test the blade profile is, NREL's S809 that's airfoil profile is shown in fig.11 .In phase II rotor rotated constantly at 72 rpm that extracted 20 kW of electrical power output. The blade pitch angel is constant 12˚ and bade has no twist. Blade span is about 5.03 meter so its wind turbine radius and blade chord is constant 0.458 meter and has no taper.

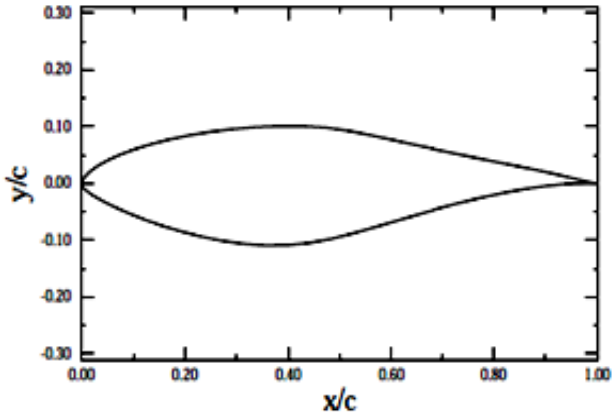

Fig.11 NREL S809 Airfoil Profile [13]

Fig.12 and fig.13 shows the comparison of computational pressure coefficients with those of the experiment, respectively in 30% and 80% span. The numerical solutions, for all turbulence model cases, are quite close to experimental data at both 80% and 30% span. It is interesting that the RNG k-ε and Spalart-Allmaras turbulence model but have result much more closely to the experimental but Spalart-Allmaras turbulence model have much better convergence than k-ε model. However at 30% span, the numerical results is not in good agreement with the experiment as much as numerical result in 80% span, but the result is good enough; again, the RNG k-ε and Spalart-Allmaras have lightly better agreement with experimental data, in 30% span, in this position we have more turbulent complication in suction side(fig.14).

Fig.14 and fig15 show the stream lines around the turbine blade in 30% and 80% span, respectively. It is seen that the flow is attached to the blade in 80% but it has stall in 3o% because of the high angle of attack in sections near the hub. And also pressure contour are shown in fig.16 and fig.17.

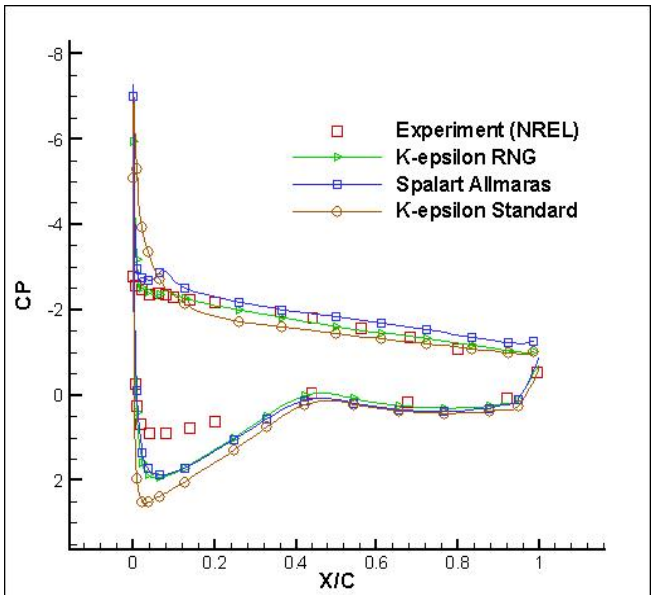

Fig.12 Pressure coefficient in 30% span at 10.5 m/s wind speed

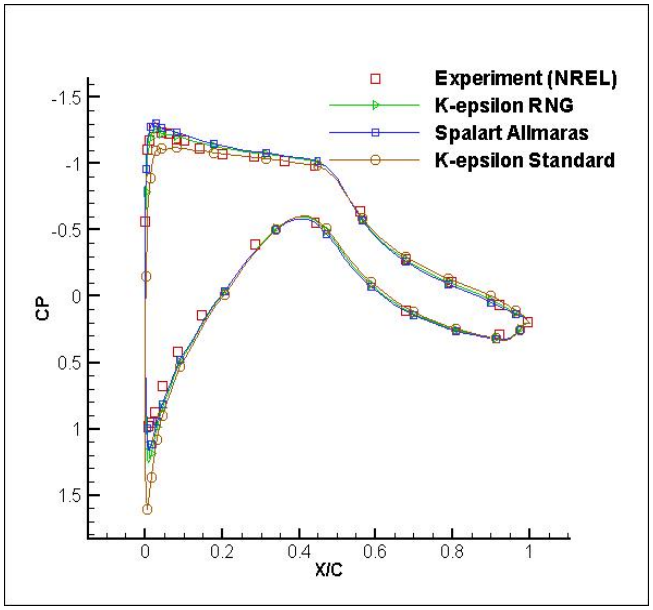

Fig.13 Pressure coefficient in 80% span at 10.5m/s wind speed

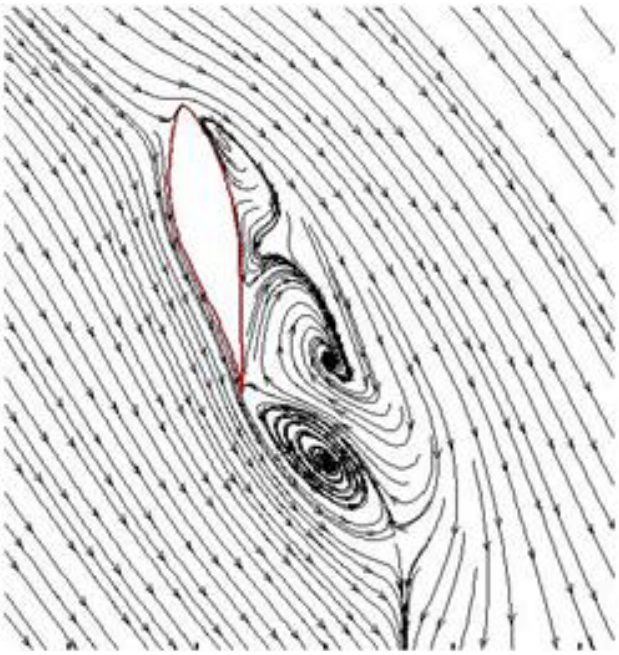

Fig.14 Streamline around the blade in 30% span at 10.5m/s wind speed

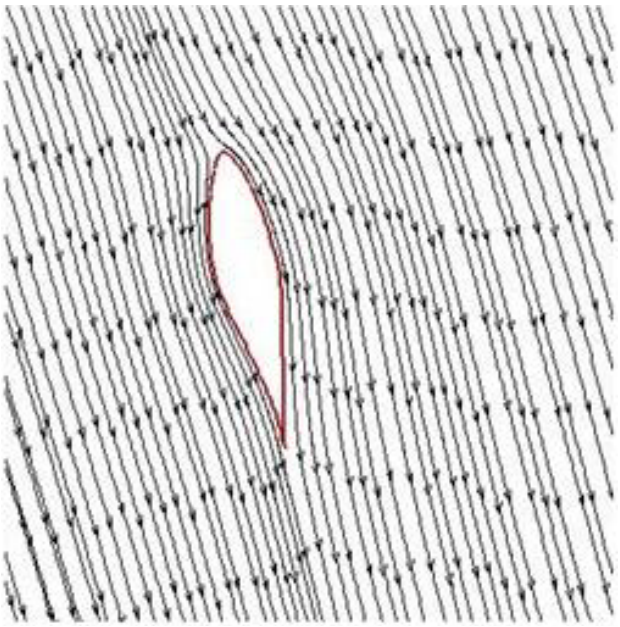

Fig.15 Streamline around the blade in 80% span at 10.5m/s wind speed

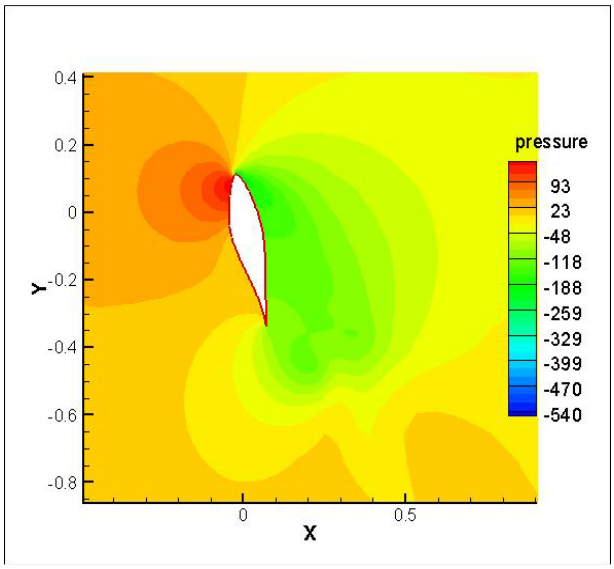

Fig.16 Pressure contour in 30% span at 10.5m/s wind speed

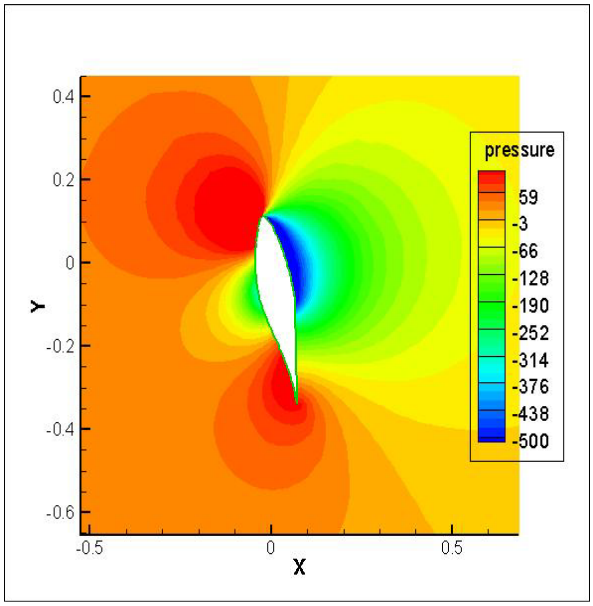

Fig.17 Pressure contour in 80% span (right) at 10.5m/s wind speed

The comparisons of rotor torques are shown in Table 2 , 3

Table1. CFD results compared with experiments at wind speed=7.2 m/s

Turbulence model	CFD	Experimental Measurements			
	Torque (Nm)	Strain gauge		Generator	
		Torque (Nm)	%Error	Torque (Nm)	%Error
Standard k-ε	241.47	286.22	-15.63	317.26	-23.88
RNG k-ε	263.66		-7.88		-16.89
Spalart-Allmaras	288.77		0.89		-8.978

Table2. CFD results compared with experiments at wind speed=10.5 m/s

Turbulence model	CFD	Experimental Measurements			
	Torque (Nm)	Strain gauge		Generator	
		Torque (Nm)	% Error	Torque (Nm)	% Error
Standard k-ε	1078.65	1207.39	-10.66	1190.04	-9.35
RNG k-ε	1254.44		3.89		5.41
Spalart-Allmaras	1309.97		8.49		10.07

Extended torque from wind turbine blades has been calculated with used of blade element theory (fig19). Fig.19 and fig.20 shows respectively, velocity and force orientation in blade section in each element.

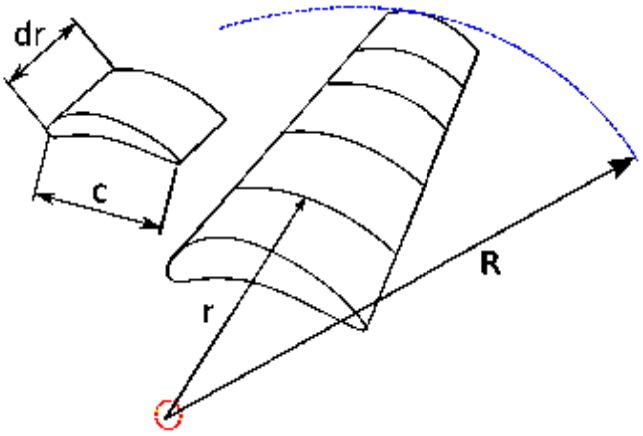

Figure 18: The Blade Element Model [14]

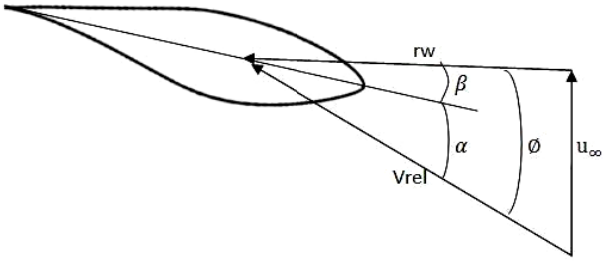

Fig.19 The velocity diagram for the blade section

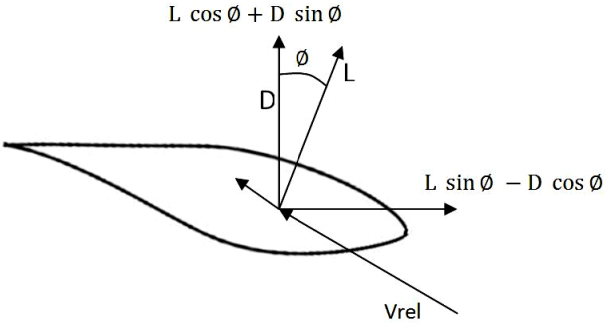

Fig.20 The velocity diagram for the blade section

Differential rotor torque in each element can be determined as:

$$dT = [L\sin\emptyset - D\cos\emptyset]r \qquad (32)$$

The overall torque is sum of the total blade elements.

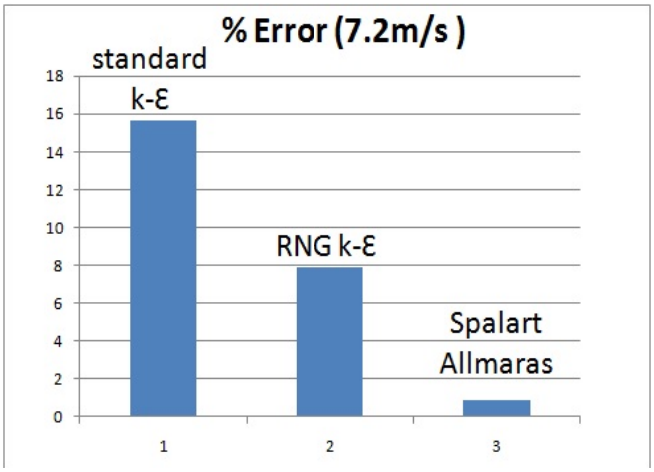

Fig .21 Absolute value error in torque calculation at wind speed 7.2 m/s

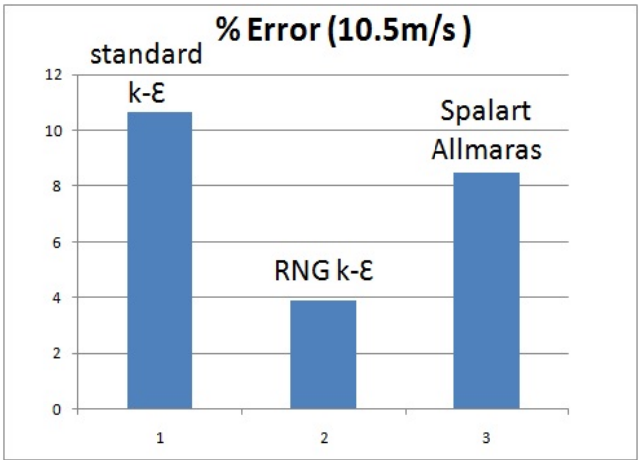

Fig.22 Absolute value error in torque calculation at wind speed 10.5 m/s

Table1 and fig.21 indicates that in low wind speed, the Spalart-Allmamaras turbulence model have incredibly high agreement with experimental data. Since, as explained in section2.2.1, the Spalart-Allmaras model was designed specifically for aerospace applications involving wall-bounded flows and it has good results for boundary layers subjected to adverse pressure gradients. In addition, the Spalart-Allmaras model is effectively a low-Reynolds-number model, requiring the viscosity-affected region of the boundary layer to be properly resolved. However, as shown in table2 and fig.22 in higher wind speed RNG k-ε turbulence has better agreement and standard k-ε model in both high and low speed has high error from experimental data the reason is, it cannot predict flow separation accurately because it neither integrates up to the wall nor does it account for modification of turbulence dissipation due to an adverse pressure gradient [16].

Furthermore, it can be seen the wake effect after wind turbine blade in CFD calculation, for example fig.23 and fig.24 shows wake effect on velocity and total pressure respectively.

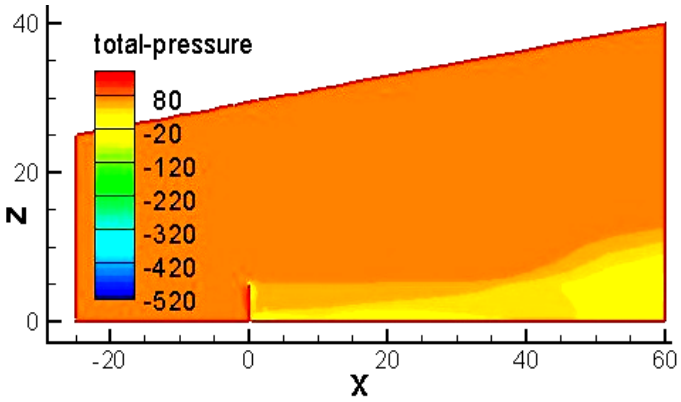

Fig.23 The wake of the wind turbine blade and its effect on total pressure

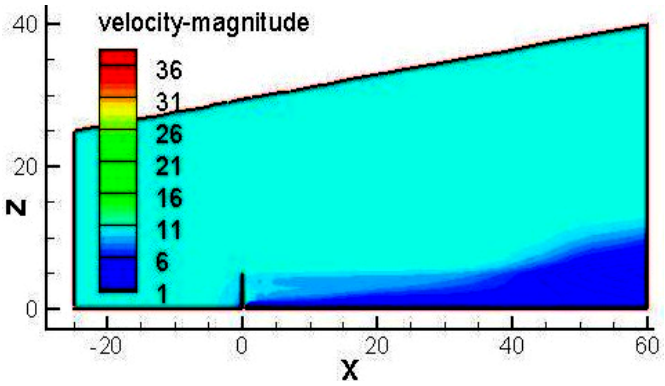

Fig.24 The wake of the wind turbine blade and its effect on the velocity magnitude

For an ideal wind turbine operating at maximum efficiency, the effective upstream area is two-thirds the swept area and the area of the wake downstream is twice the area swept by the rotor.

However, conserving angular momentum necessitates rotation of the wake if the rotor is to extract useful torque. Moreover, the flow behind the rotor will rotate in the opposite direction as the rotor in reaction to the flow imparting torque on the rotor as shown in Fig.25:

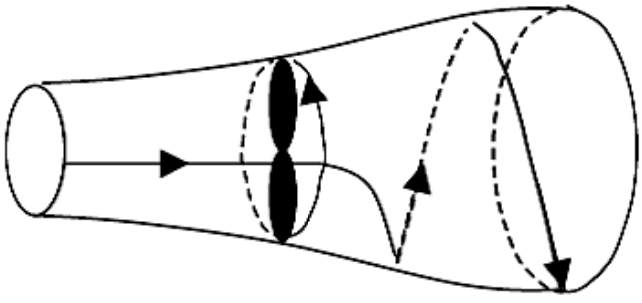

Fig.25 The Schematic view of the wake rotation

Since the wake is now rotating, it exhibits rotational kinetic energy that reduces the amount of available energy that can be extracted as useful work, this is the reason that magnitude velocity and total pressure reduce, as shown in fig.23 and fig.24

4 Conclusion

CFD calculation of HAWT blade aerodynamic with rectangular full structure grid was carried out and the evaluation of three turbulence model had been done to predict pressure coefficient and power of horizontal axis wind turbine for two wind speeds.
Both Spalart-Allmaras and RNG k-ε turbulence model have reasonable results and with good agreements with experimental data. We comments in low wind speed Splart-Allmaras model gives much more better result and in high wind speed RNG k-ε turbulence model has better agreement with experimental data. However the Standard k-ε results was not good enough to predict HAWT torque accurately. In addition, Splart-Allmaras model has much better convergence and low computing cost.

References:

[1]Tony Burton,David Sharpe,Nick Jenkins,Ervin Bossanyi , *Wind Energy Handbook ,* JOHN WILEY & SONS, LTD, 2001

[2] Martin O. L. Hansen, *Aerodynamics of Wind Turbines*, Second Edition, published by Earthscan in the UK and USA in 2008

[3] Jonkman JM. , Modeling of the UAE wind turbine for refinement of FAST_AD, NREL/TP-500-34755. Colorado: *National Renewable Energy Laboratory*; December 2003

[4] T. J. Barth and D. Jespersen , The design and application of upwind schemes on unstructured meshes, *Technical Report AIAA-89-0366,* AIAA 27th Aerospace Sciences Meeting, Reno, Nevada, 1989.

[5] Patankar SV, *Numerical heat transfer and fluid flow,* New York: Hemisphere Publishing Corperation, Taylor & Francis Group; 1980.

[6] Batchelor GK. , *An introduction to fluid dynamics*. Cambridge: Cambridge University Press; 1967.

[7] Spalart, P. R., and Allmaras, S. R., "A One-Equation Turbulence Model for Aerodynamic Flows," *AIAA Paper 92-0439*, 1992.

[8] Ferziger, J.H. and Peric, M*., Computational Methods for Fluid Dynamics*, Springer, 1996

[9] Chalothorn Thumthae, Tawit Chitsomboon "Optimal angle of attack for untwisted blade wind turbine" *Renewable Energy 34* (2009) 1279–1284

[10] Colleen D.Scott-Pomerant, the *K-Epsilon Model in Theory of Turbulence*, University of Pittsburgh, 2004

[11] J.Y.Luo, R.I.Issa, and A. D. Gosman, Prediction of Impeller-Induced Flows in Mixing Vessels Using Multiple Frames of Reference, In *IChemE Symposium Series*,number 136, pages 549–556, 1994

[12] Simms DA, Hand MM, Fingersh LJ, Jager DW. Unsteady aerodynamics experiment Phases II-IV test configurations and available data campaigns. Colorado: *National Renewable Energy Laboratory*; July 1999.

[13] J. L. Tangler , NREL Airfoil Families for HAWTs, *National Renewable Energy Laboratory* 1617 Cole Boulevard Golden,Colorado 80401-3393, updated AWEA 1995.

[14] Grant Ingram "Wind Turbine Blade Analysis using the Blade Element Momentum Method" School of Engineering, Durham University, December 13, 2005

[15] R.S. Amano, R.J. Malloy, "CFD Analysis on Aerodynamic Design Optimization of Wind Turbine Rotor Blades" *World Academy of Science, Engineering and Technology* 60 2009

[16] David Hartwanger* and Dr Andrej Horvat ,*3D MODELLING OF A WIND TURBINE USING CFD***,** NAFEMS Conference 2008, United Kingdom.